The influence of lithospheric flexure on magma ascent at large volcanoes on Venus

Patrick J. McGovern,[1] M. Elise Rumpf,[2] and James R. Zimbelman[3]

Received 7 June 2013; revised 11 October 2013; accepted 21 October 2013; published 27 November 2013.

[1] Large volcanoes on Venus exert large vertical loads on the lithosphere, which responds by deflecting downward. Stresses induced by this lithospheric flexure can have a strong influence on magma ascent pathways from the mantle source region to the surface. Here we propose that flexural stresses exert control over the shapes of volcanic edifices on Venus, applying criteria for magma ascent expressed in terms of stress orientations (can vertical dikes form?) and gradients (is magma squeezed upward or downward in a vertical dike?) to determine favored magma ascent paths and locations. For conical edifices emplaced on lithosphere with high elastic thickness T_e, (e.g., > 40 km) both sets of magma ascent criteria are satisfied over the entire lithosphere, allowing essentially unimpeded ascent of magma to the surface and the formation of relatively steep edifices. However, for lower values of T_e, high adverse stress gradients tend to cut off magma ascent beneath the summit, instead favoring lateral transport of magma at depth to distal regions with gentler stress gradients, resulting in domical edifice shapes. At the lowest values of T_e (< 10 km), large short-wavelength deflections of the lithosphere tend to produce narrow and widely spaced zones of magma ascent: Such zones may produce annular ridges of volcanic material, thereby generating forms characteristic of a subset of features known as "coronae" on Venus. Another subset of coronae may form by intrusive-based generation of annular fractures at the edge of the summit region of domical edifices, as proposed for Alba Mons on Mars.

Citation: McGovern, P. J., M. E. Rumpf, and J. R. Zimbelman (2013), The influence of lithospheric flexure on magma ascent at large volcanoes on Venus, *J. Geophys. Res. Planets*, *118*, 2423–2437, doi:10.1002/2013JE004455.

1. Introduction

[2] Large volcanic edifices constitute a significant portion of the geologic record of Venus, as revealed by radar-based imaging and ranging of the surface of that planet [e.g., *Head et al*., 1992; *Crumpler et al*., 1997]. In particular, synthetic aperture radar images collected from the Magellan mission [*Saunders et al*., 1992] revealed volcanic flows, faults, and vents in unprecedented resolution, greatly advancing our ability to understand the evolution of large volcanic constructs on Venus. Furthermore, the shapes and sizes of the features were constrained by Magellan altimetry data. More than 150 large volcanoes [*Head et al*., 1992; *Crumpler et al*., 1997; *McGovern and Solomon*, 1998] have been identified. In general, these volcanoes comprise a topographic edifice of order several kilometers in height and a surrounding apron of flows fanning out from the center over extremely low slopes; the apron flows likely fill topographic lows (moats) resulting from lithospheric flexure [*McGovern and Solomon*, 1997]. The long distances covered by individual lava flows (up to hundreds of km) indicate relatively low magma viscosity, pointing toward a basaltic composition. Each volcano likely comprises thousands of such flows. A fraction of the volcanoes identified in *McGovern and Solomon* [1998] were also assigned to the morphological category "corona", based on the existence of annular topographic and tectonic signatures [*Stofan et al*., 1992; *Stofan et al*., 2001].

[3] The growth of large volcanic edifices on Venus poses a volcanological riddle. *McGovern and Solomon* [1998] pointed out that large edifices on Venus exert large loads on the lithosphere, and this loading generates large compressional stresses within the upper lithosphere and edifice. Using finite element models of incrementally loaded, conical volcanic edifices coupled to the underlying lithosphere, these workers illustrated how compression increases with height to produce a zone of high-magnitude horizontal compression in the proximal upper lithosphere and into the edifice. Using the well-known ascent criterion based on principal stress orientations [*Anderson*, 1951], such a stress state would inhibit magma ascent in dikes, instead favoring lateral transport in subhorizontal sills. This ascent difficulty is compounded

Additional supporting information may be found in the online version of this article.

[1]Lunar and Planetary Institute, Universities Space Research Association, Houston, Texas, USA.
[2]Hawaii Institute of Geophysics and Planetology, University of Hawaii, Manoa, Hawaii, USA.
[3]Center for Earth and Planetary Studies, MRC 315, Smithsonian Institution, Washington, District of Columbia, USA.

Corresponding author: P. J. McGovern, Lunar and Planetary Institute, Universities Space Research Association, Houston, TX 77058, USA. (mcgovern@lpi.usra.edu)

2169-9097/13/10.1002/2013JE004455

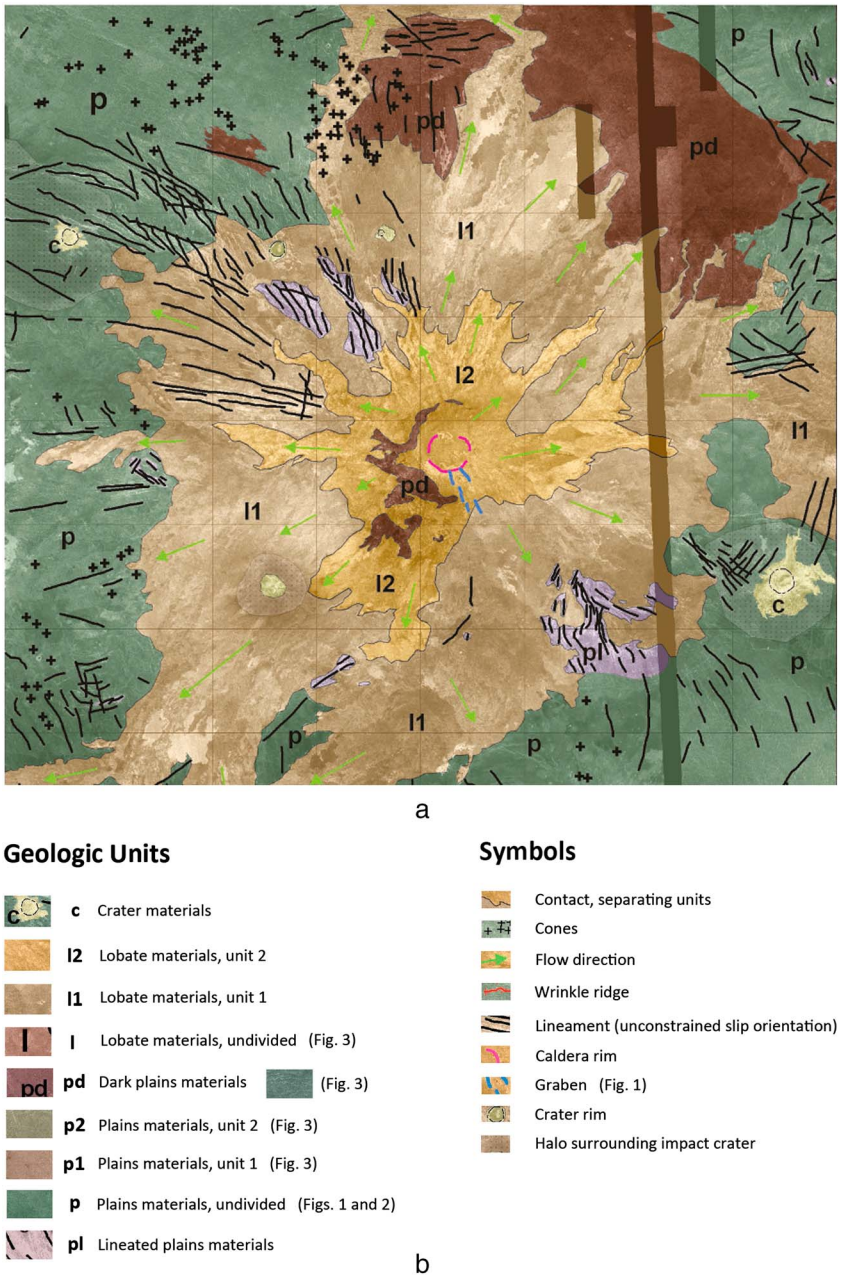

Figure 1. (a) Geologic map for the volcano Sif Mons (21.7°N 351.8°E). Grid lines are at 1° intervals: 1° of latitude equals about 105 km. Base map image obtained from USGS Map-a-Planet website (http://www.mapaplanet.org). (b) Legend: Basic units, youngest to oldest, c, impact crater and ejecta; l2, lobate flows, upper unit (later-stage effusion from the caldera, which likely buried the southern caldera rim); l1, lobate flows, lower unit (early stage effusion, plus lobate flows removed from the volcano itself); pd, dark plains (radar-dark plains, some associated with the impacts); p, regional plains (undivided); and pl, lineated plains (oldest exposed materials, with one main lineation direction, unlike tesserae). Symbols are individual cones (plus), flow direction for lobate materials (green arrows), wrinkle ridges (red line with hachures), caldera rim (pink line with hachures), and lineaments (thick black lines: could be graben, fault, or joint; sense of movement not resolved). Blue lines are graben (south of the caldera rim) and patterns around craters are radar-darkened shock halo zones associated with the impact event [e.g., *Zahnle*, 1992].

when the physics of magma transport in dikes is considered [*Rubin*, 1995]; increasing compression with height tends to squeeze upper dike tips shut. On the other hand, a stress state with the opposite condition (increasing extension with height) could allow for rapid magma ascent [*Rubin*, 1995].

[4] The physics of magma ascent in dikes has been the subject of numerous studies [e.g., *Lister and Kerr*, 1991; *Rubin*, 1995; *Gudmundsson*, 2002, 2006; *Ito and Martel*, 2002]. Others have considered magma chamber pressurization beneath small (relative to Venus volcanoes) volcanic edifices

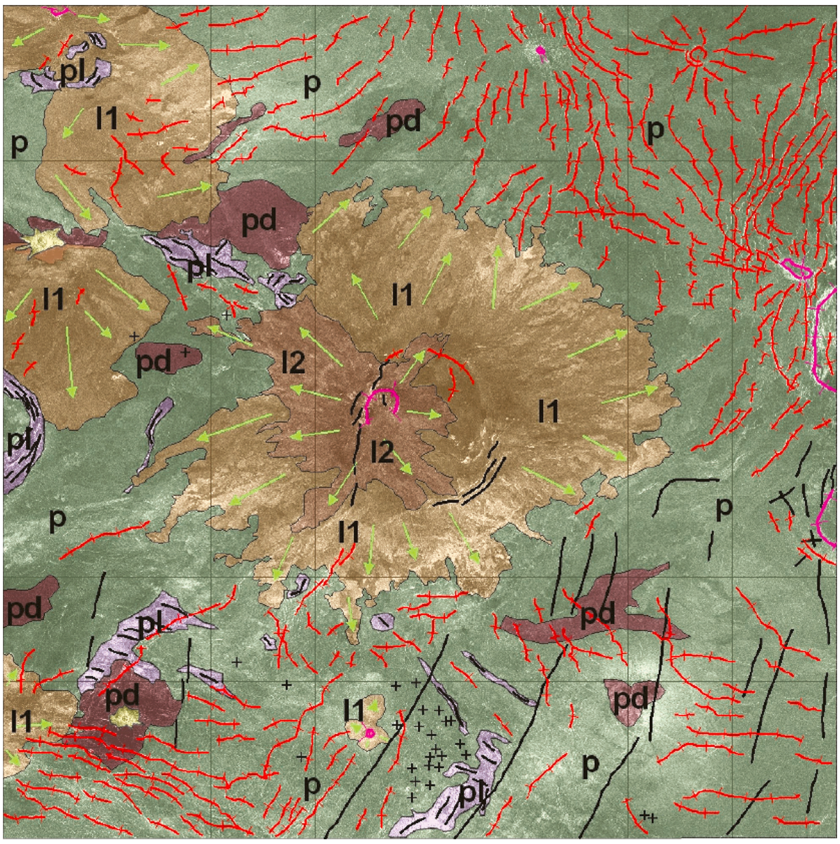

Figure 2. Geologic map, as in Figure 1, for the volcano Kokyanwuti Mons (35.5°N 211.6°E: plot bounds 31.5–39.5°N, 207.5–215.5°E).

and the orientations of intrusions emanating from them [e.g., *Pinel and Jaupart*, 2003, 2004; *Grosfils*, 2007; *Long and Grosfils*, 2009; *Hurwitz et al*., 2009]. However, none of these studies explicitly addressed flexural stress states, which can provide stress magnitudes well in excess of those from simple compression of the substratum and significantly different distributions of stress with depth. Edifice stresses induced by flexure beneath conical or wedge-shaped edifices were calculated by *McGovern and Solomon* [1993, 1998], *Borgia* [1994], *van Wyk de Vries and Matela* [1998], and *McGovern et al*. [2001]. The effects of subvolcano lithospheric stress state on ascent have also been explored [*ten Brink and Brocher*, 1987; *McGovern and Solomon*, 1993, 1998; *Hieronymus and Bercovici*, 2001a, 2001b; *Pritchard et al*., 2006; *McGovern*, 2007]. The effects of stresses from lithospheric flexure on magma chamber failure and dike propagation at large volcanoes on Venus were demonstrated by *Galgana et al*. [2011, 2013].

[5] In this paper, we explore the interactions of edifice loading, lithospheric stress, and magma ascent at large volcanoes on Venus. We examine several large volcanoes on Venus that are representative of distinct edifice shapes: a simple cone (Sif Mons, Figure 1), a domical shape (Kokyanwuti Mons, Figure 2), and a volcanic member of the morphologic class corona with annular topography (Aruru Corona, Figure 3). We calculate stresses from lithospheric loading by edifices with these shapes. We evaluate lithospheric stresses via two criteria for magma ascent, the "orientation" [*Anderson*, 1936] and "gradient" [*Rubin*, 1995] criteria, in order to predict preferred and proscribed locations of magma ascent as a function of radial distance from the center of the edifice. We demonstrate that the thickness of the (idealized) elastic lithosphere T_e interacts strongly with edifice shapes to produce characteristic modes of magma ascent that in turn can reinforce the shapes, and that therefore, each shape has a characteristic T_e range associated with it. We discuss the implications of these findings for the volcano-tectonic evolution of large edifices on Venus and for regional and global thermal evolution of Venus.

2. Structure of Large Volcanic Edifices on Venus

[6] Sif Mons (Figures 1a and 4; center at 21.7°N 351.8°E, topographic edifice radius $r_{ed} = 142$ km, flow apron radius $r_{fl} = 300$ km, height above base $h = 2.2$ km [*McGovern*, 1996]) is an example of a conical volcanic edifice with radial flows covering the topographic edifice and surrounding flow apron [*McGovern and Solomon*, 1997]. The central edifice is covered by an annulus of radially textured flows (Figure 1a). These flows are superposed on mottled bright plains consisting of 150–200 km long, 15–20 km wide flows also radial in orientation [*Senske et al*., 1992]. The mottled bright plains unit is believed to represent an early stage of high magmatic flux, based on its broad lateral and radial extent [*Senske et al*., 1992]. The narrow summit region exhibits an arcuate structure that may be a partially buried caldera of diameter ~40 km [*Copp and Guest*, 2007]. Several graben radiate outward from the southeast margin of the caldera, perhaps delineating the surface traces of radial dikes (Figure 1a). Several radial pits and pit chains are seen at the southeast

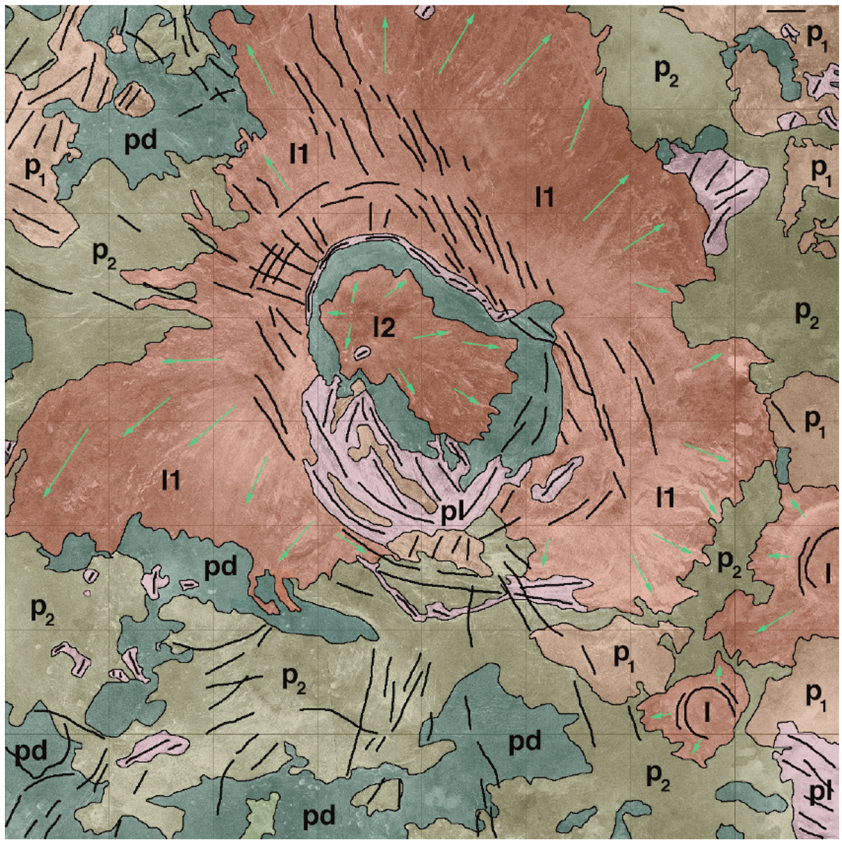

Figure 3. Geologic map, as in Figure 1, for annular volcano Aruru Corona (9.45°N 262.4°E: plot bounds 5–13°N 258–266°E). Legend: base units and symbols are like the Sif map (Figure 1) except that the regional plains have two subdivisions (p2, locally superposed on p1), and an undivided lobate flows unit (l) is included.

margin of the caldera [*Senske et al*., 1992]; the pit chains are similar in size and orientation to those observed in the western Galapagos Islands [*Chadwick and Howard*, 1991]. The northwest margin of the caldera appears to be flooded by lavas overflowing the northwest rim. Radially oriented fractures, believed to be long, narrow graben, are seen on the northwest flank [*Senske et al*., 1992]. Extensional faulting is seen between lobes of lava flow units in the flow apron; the latter appear to embay the former, suggesting that the faulting occurred before volcano formation, or at least in an early stage of it. The extensional faults are roughly radial to the summit region, consistent with emplacement via radial diking.

[7] Kokyanwuti Mons (35.5°N 211.6°E, r_{ed} = 165 km, r_{fl} = 200 km, h = 1.8 km [*McGovern*, 1996]) exhibits a domical profile, with a nearly flat summit region and gently sloping outer flanks (Figure 4). The summit has a fairly uniform radar-dark surface; the subdued flow unit definition here contrasts with the vibrant, well-defined digitate flows with varying brightness in the radar backscatter, radiating outward in the flow apron (Figure 2). Tectonic lineaments, roughly circumferential to the summit, are seen on the northwest and southeast margins of the summit plateau and lower on the flank (the sense of movement cannot be determined, so they may be extensional or compressional in nature), and in the southeast, they are adjoined by pits arranged along circumferential trends. The region inside the tectonic annulus is very flat, giving the volcano a domical shape (Figure 4). Radially oriented tectonic features are not evident, except for two parallel sets of fractures diverging from the southwest corner of the annulus into the surrounding terrain (Figure 2). This divergence may indicate interaction of a regional stress field with edifice stresses. Radially oriented flows extend a great distance to the north and west. High regional topography to the south and east of the edifice re-

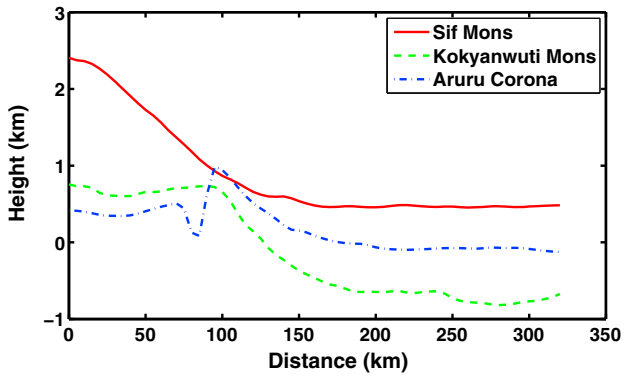

Figure 4. Radial topographic cross sections for Sif Mons (center 21.7°N 351.8°E, azimuth 30°), Kokyanwuti Mons (center 35.5°N 211.6°E, azimuth 15°), and Aruru Corona (center 9.45°N 262.4°E, azimuth 30°) from Magellan altimetry [*Ford and Pettengill*, 1992].

Table 1. Parameter Values, After *McGovern and Solomon* [1998]

Parameter	Value
E	1×10^{11} Pa
v	0.25
ρ_{volcano}	2800 kg/m^3
ρ_{mantle}	3300 kg/m^3
g	−8.87 m/s^2

stricts the extent of apron flows in those directions. An arcuate structure about 30 km in diameter on the northwest side of the summit region (Figure 2), just inside the broader lineament arc, may be a caldera.

[8] Aruru Corona (Figure 4; 9.45°N 262.4°E, $r_{\text{ed}} = 260$ km, $h = 1.4$ km) displays characteristic annular topographic edifice profiles (Figure 4), voluminous flank and apron flow units, and abundant fractures with both radial and circumferential orientations (Figure 3). Numerous lava flows appear to have resurfaced the outer slope of the annulus. Flows emanating from the outer surface of the edifice form a flow apron similar to those seen surrounding large edifices with domical and conical shapes (e.g., Figures 1a and 2). Some flows appear to have emanated from the inner slope as well, covering the interior low region. Tectonic lineaments have a predominantly circumferential orientation on the upper part of the outer surface of the annulus (units pl and pd), with mixed circumferential and radial orientations further down the outer flank (Figure 3). Distal fractures in the l1 flow unit appear to converge on a roughly north-northwest-/south-southeast-trending regional-scale alignment, perhaps reflecting regional stress fields.

3. Magma Ascent Criteria

[9] Here we summarize two types of criteria for magma ascent through the lithosphere in vertical dikes. The first type of criterion simply states the finding of *Anderson* [1951] that intrusions tend to form perpendicular to the least compressive principal stress. This "stress orientation" criterion is

$$\Delta\sigma_{\text{y}} + \sigma_{\text{local}} > 0 \tag{1}$$

where is defined as the difference of horizontal normal stress perpendicular to the dike and vertical normal stress ($\sigma_{\text{y}} - \sigma_{\text{z}}$; this is termed the "tectonic" stress by *Rubin* [1995]) and σ_{local} is a local variation in stress due to factors such as local inhomogeneities and modifications to the lithosphere, regional-scale stress fields, and reductions in stress from yielding at the top and bottom of the lithosphere. In axisymmetry, there are two horizontal normal stresses: the radial (σ_{rr}) and the "hoop" ($\sigma_{\theta\theta}$), the latter oriented perpendicular to the symmetry (r-z) plane.

[10] A second, less well-known type of ascent criterion is based on pressure balance in vertical dikes. *Rubin* [1995] summarizes three sources of pressure available to drive magma flow in vertical dikes (his equation (7), modified to account for our "tension positive, z positive upward" sign conventions):

$$(\mathrm{d}P/\mathrm{d}z + \rho_{\text{m}}g) = \mathrm{d}\Delta\sigma_y/\mathrm{d}z + \mathrm{d}\Delta\mathrm{P}/\mathrm{d}z - \Delta\rho g, \tag{2}$$

where P is magma pressure, ρ_{m} is magma density, $\Delta\rho$ is host rock density ρ_{r} minus magma density ρ_{m}, ΔP is local excess magma pressure, and g is the surface gravity of Venus. The left-hand term in equation (2) is a factor in the relation for mean magma flow velocity u_z given laminar flow (equation (4) of *Rubin* [1995])

$$u_z = (1/3\ \eta)w^2(\mathrm{d}P/\mathrm{d}z + \rho_{\text{m}}g), \tag{3}$$

where η is the magma viscosity and w is the dike half thickness. For z defined positive upward (note: this choice makes g negative), the quantity $\mathrm{d}P/\mathrm{d}z + \rho_{\text{m}}g$ must be positive to obtain magma ascent (flow in the positive z direction). In practice, when flexure is significant (see below), the term $\mathrm{d}\Delta\sigma_{\text{y}}/\mathrm{d}z$, the vertical gradient of tectonic stress, dominates the pressure balance. Substituting equation (2) into equation (3), we get

$$u_z = (1/3\ \eta)w^2\left(\mathrm{d}\Delta\sigma_y/\mathrm{d}z + \Delta\mathrm{PG}\right), \tag{4}$$

where we have collected the local excess magma pressure gradient and buoyancy terms into the term ΔPG, and the stress gradient criterion for ascent becomes $\mathrm{d}\Delta\sigma_{\text{y}}/\mathrm{d}z + \Delta PG > 0$. In general, the dominant $\mathrm{d}\Delta\sigma_{\text{y}}/\mathrm{d}z$ term must be positive for magma ascent, i.e., differential compression must decrease with height; otherwise, by equation (4) (neglecting ΔPG for the moment), magma would be forced downward rather than upward. Thus, even though principal stress orientations in the lower lithosphere are consistent with vertical dikes, the upward increase in horizontal compression will in effect "squeeze off" the dikes, preventing magma ascent beyond the lower lithosphere. In other words, the magma is effectively "negatively buoyant" [*Rubin*, 1995].

4. Method

[11] We calculate deflections and tectonic stresses $\Delta\sigma_{\text{y}}$ due to volcanic loading on the lithosphere using the elastic "thick-plate" analytic flexure solution of *Comer* [1983], in axisymmetric geometry. The shape of a volcanic edifice is broken down into a series of harmonics via the Hankel transform (the axisymmetric equivalent of the Fourier transform), and the flexural responses from each harmonic are superposed to get the final solution. We considered three edifice shapes, starting with a cone. A truncated or flat-topped cone, intended to represent a domical edifce, was generated via subtraction of a small cone from a large one [*Comer*, 1983], and a further subtraction generated an annular edifice that resembles a subset of the Venusian coronae. Volcanic loads in these shapes, of given height and radius, were applied to the lithosphere. We assumed crustal and volcano densities ρ_{crust} and ρ_{volcano} of 2800 kg/m^3 and a mantle density $\rho_{\text{mantle}}$of 3300 kg/m^3 [e.g., *McGovern and Solomon*, 1998]. Lithospheric Young's modulus E and Poisson's ratio v were taken to be 1×10^{11} Pa and 0.25, respectively (Table 1). The flexural depression was assumed to be filled with a material of the same density as that of the volcano. The response of the lithosphere to a load is controlled by the thickness of the elastic layer, T_{e}, which was the assigned values ranging from 5 to 60 km. The code calculates the radial normal stress σ_{rr} and the out-of-symmetry-plane or hoop normal stress $\sigma_{\theta\theta}$. For a given edifice, deflections and stresses were calculated as functions of radius from the axis of symmetry and of depth within the plate [*Comer*, 1983]. Stress gradients were calculated from the stresses at the top and bottom of the lithosphere and T_{e}.

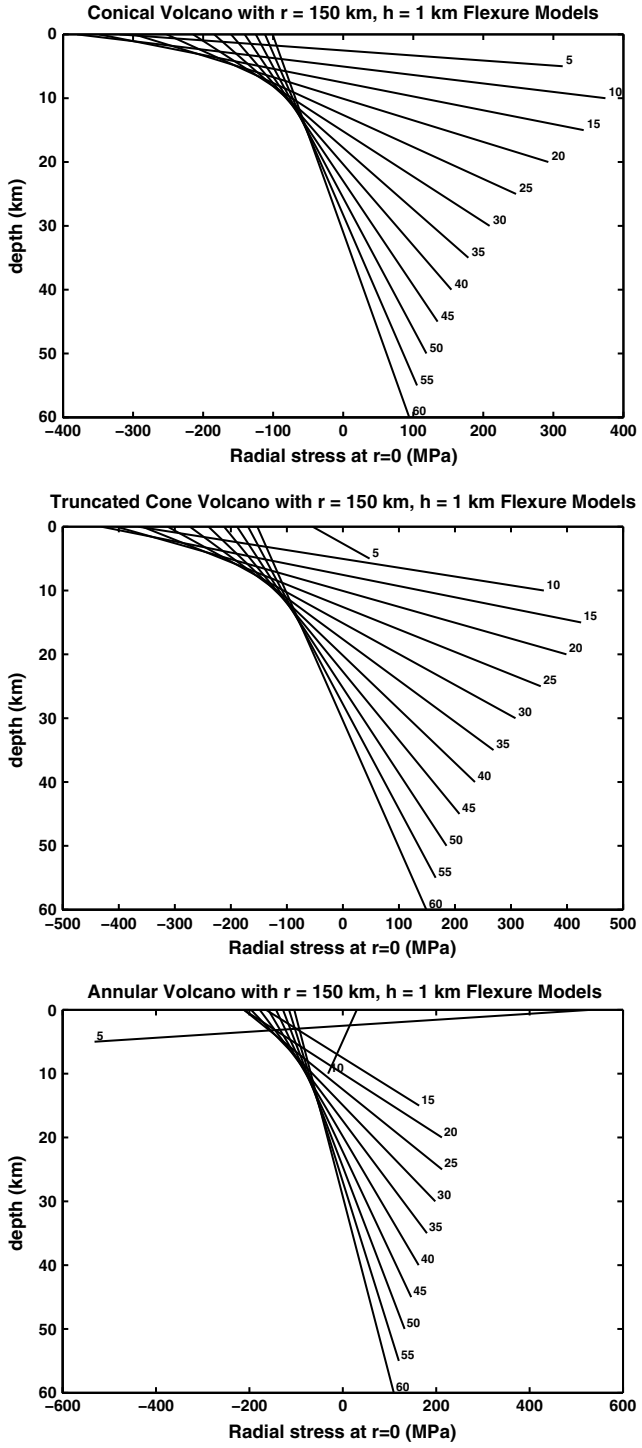

Figure 5. Radial normal stress σ_{rr} beneath the center of volcanic edifices ($r = 0$) versus depth z in the lithosphere for three edifice shapes, all with maximum height 1 km and radius 150 km. Elastic thickness T_e values range from 5 km to 60 km in 5 km increments: Stress curves are labeled with the corresponding T_e value. (a) Conical edifice, (b) truncated cone or domical edifice, and (c) annular edifice.

[12] For a given vertical lithospheric stress distribution at a given r coordinate, we apply the stress orientation and stress gradient ascent criteria of the previous section to determine whether or not magma can ascend at that location. Given that in elastic lithospheres the stress extrema are at the top and bottom of the lithosphere, we apply the stress orientation type criterion at those locations. For the elastic case, the calculated stress gradient is constant throughout the thickness of the lithosphere and is used to evaluate the stress gradient type criterion. Thus, in practice, there are three ascent criteria to be met.

[13] In practice, the "dipole" nature of flexural stresses means that one of the stress orientation criteria will not be satisfied. However, the stress states calculated here do not account for factors that would mitigate conditions nominally adverse to magma ascent. To account for these mitigating factors, we apply stress and stress gradient "thresholds" to the stresses calculated by the models described above, in the form of σ_{local} for the stress orientation criterion and ΔPG for the stress gradient criterion. The thresholds allow ascent criteria to be satisfied for modestly adverse values of stress (negative horizontal differential stress) and stress gradient (negative $d\Delta\sigma_y/dz$).

[14] For the stress orientation type criterion, the threshold accounts for phenomena that reduce compressive stresses. Phenomena that directly modify the idealized elastic stress profile in the lithosphere include brittle failure (faulting), ductile flow (yielding), fracture ahead of dike tip, thermomechanical erosion [*Hieronymus and Bercovici*, 2001a, 2001b], and compressive stress reduction due to the edifice taking up part of flexural load [*McGovern and Solomon*, 1993, 1998]. Also, the stress profile can be changed by intrusion of material into the midlithosphere, as at the Island of Hawaii [*McGovern*, 2007], because newly emplaced material feels only the effects of subsequent loading [*McGovern and Solomon*, 1993, 1998]. Underplating or other buoyant support [e.g., *ten Brink and Brocher*, 1987; *Wolfe et al.*, 1994] counteracts subsidence from edifice loading, thereby reducing stress. The latter effect is most significant at low T_e. For stress gradient criterion, the threshold accounts for the stress-mitigating effects listed above plus magma overpressure and buoyancy.

5. Results

[15] Figure 5 illustrates how lithospheric flexure interacts with edifice shape to control the state of stress in the lithosphere. This figure shows the radial normal stress as a function of depth beneath the central axis ($r = 0$) for edifices with radius = 150 km in three shapes: conical, domical, and annular, for varying T_e. For the conical edifice (Figure 5a), maximum stress magnitudes at the top and bottom of the lithosphere generally increase with decreasing T_e, although at the very smallest values of T_e they start to decrease, due to the shift of flexural accommodation to the margin of the load that relieves stress at the axis [see also *McGovern and Solomon*, 1998, Figure 10]. Over the entire range of modeled elastic lithosphere thickness T_e (5–60 km), conical and truncated cone (domical) volcanoes show large negative $d\Delta\sigma_y/dz$ and large compressive (also negative) stresses at the top of the lithosphere, with one exception at $T_e = 5$ km for the domical edifice (Figure 5b). Both of these conditions would halt magma flow into the edifice, demonstrating the growth problem for conical edifices first pointed out by *McGovern and Solomon* [1993]. For an annular load, however, conditions can be much more favorable for magma ascent. At large T_e,

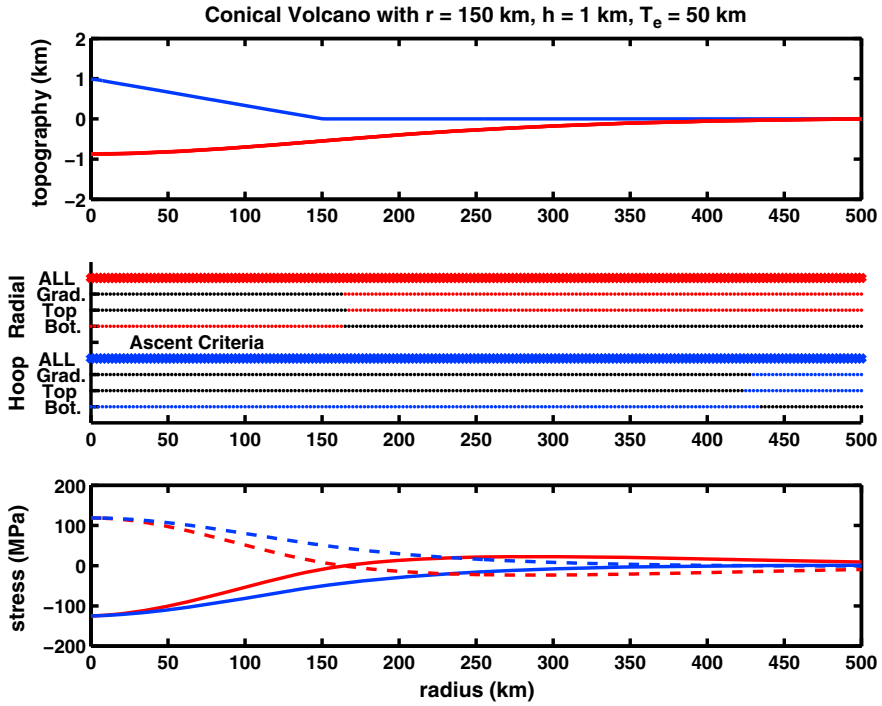

Figure 6. Flexure solutions versus radius for volcanoes with conical edifice, with peak height 1 km and radius 150 km, for $T_e = 50$ km. Stress threshold $\sigma_{local} = 150$ MPa, stress gradient threshold $\Delta PG = 6$ MPa/km. (top) Edifice topography (blue) and surface flexure (red). (middle) Ascent criteria for radial (red) and tangential (blue) normal stresses versus radius. Locations where individual criteria (stress at top and bottom of and stress gradient within lithosphere, labeled "Top", "Bot.", and "Grad.", respectively) are satisfied are shown with thin dot symbols, and locations where the total ascent criteria are satisfied (the intersection of the individual criteria, satisfied if and only if each individual criterion is satisfied) are shown with thick "cross" symbols. For an individual criterion, zones where the criterion is satisfied outright are shown in the proper color, and zones where the criterion is only satisfied by falling within a threshold are shown in black. (bottom) Radial (red) and tangential (blue) normal stresses for top (solid line) and bottom (dashed line) of elastic lithosphere. Note that in the absence of significant membrane stress components, the stress gradients in our models have essentially the same shape as the upper lithosphere (solid) stress curves, with magnitudes obtainable by dividing by $T_e/2$.

the stresses and gradients are similar in sign and magnitude to those for the other edifice shapes, but as T_e is reduced, stresses and gradient magnitudes are lower than the conical case (Figure 5c). Between $T_e = 15$ km and $T_e = 10$ km, the gradient switches sign, and the least compressional stress moves from the bottom to the top of the lithosphere (Figure 5c). This creates a favorable environment for magma ascent, although the problem of compression now switches to the lower lithosphere.

[16] We apply the ascent criteria to flexural stresses calculated as functions of radius and depth, in order to predict the radius values at which magma ascent is allowed (Figures 6–8). In axisymmetry, there are two important horizontal normal stresses, namely, the radial stress and the out-of-plane, or hoop stress. We determine the three ascent criteria for both of these stresses as functions of radius. The regions where all criteria are met for a given normal stress are marked with thick lines in Figures 6–8. For the conical volcano of Figure 5a at $T_e = 50$ km, stresses and stress gradients are within thresholds of $\sigma_{local} = 150$ MPa and $\Delta PG = 6$ MPa/km, respectively, resulting in satisfaction of the ascent criteria at all radius values (Figure 6). Similar results are seen for domical and annular edifices of the same height (in the supporting information Figures S1 and S2), although for the domical edifice there is a central cutoff in the center where the gradient and lithosphere top ascent criteria are not satisfied, likely due to its greater volume than for the other geometries.

[17] If the lithospheric thickness is reduced to 25 km, elevated lithosphere top stresses and stress gradients near the center of the load prevent the ascent criteria for both horizontal normal stresses from being satisfied there for all load geometries (Figures 7, S3, and S4). Note that in all cases, radial stresses start to satisfy the ascent criteria at a closer radial distance than the tangential stresses.

[18] If T_e is further reduced to 5 km, substantial differences start to appear in the responses to different load shapes. For an annular load (Figure 8), stresses are very high in magnitude and oscillate rapidly with increasing r. The flexural response conforms to the annular load shape with regions of high curvature (and stress) at the inner and outer margins of the annulus. For the radial stresses, there are two narrow zones that satisfy the ascent criteria on opposing flanks of the edifice, with shutoffs between and on either side

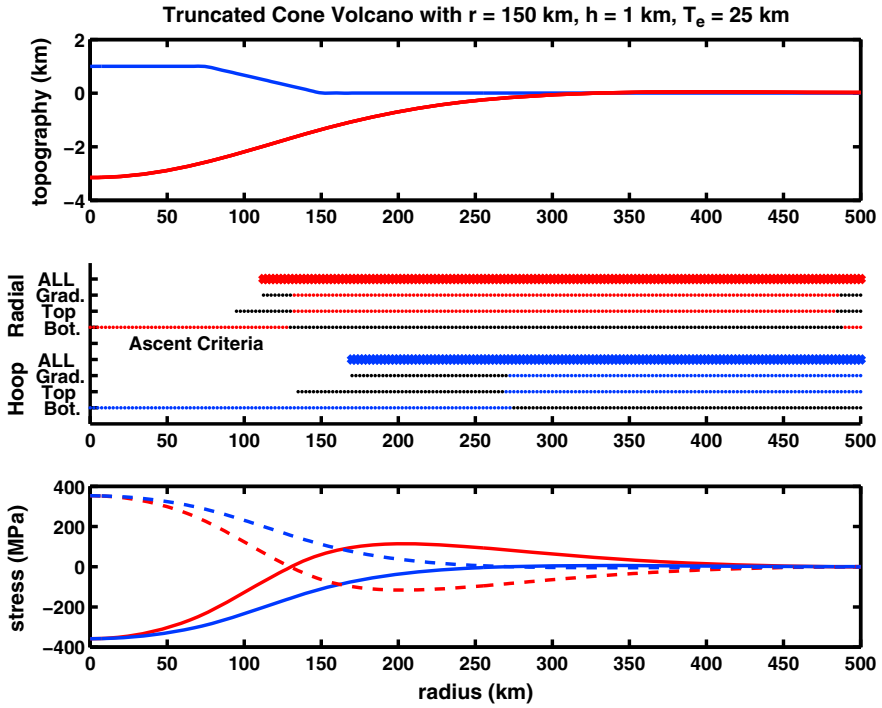

Figure 7. Flexure solutions versus radius for volcanoes with truncated cone (domical) edifice, as in Figure 5, for $T_e = 25$ km.

(including central). The usual far-field zone of allowed ascent occurs beyond the outermost cutoff. For tangential stresses, there is one inner edifice zone (slightly offset from the corresponding zone for radial stresses) and the far-field zone. In contrast, a conical edifice produces central shutoffs and distal ascent zones (Figure S5) that strongly resemble the cases with thicker T_e (Figure 6, Figure S3). The domical edifice produces an intermediate response, with a narrow lower flank ascent zone between central and distal shutoffs, and the far-field ascent zone for radial stresses, but simply the latter with a central shutoff for the tangential stresses (Figure S6).

[19] An examination of how stresses vary with T_e can illuminate the way the two magma ascent criteria interact. For a conical volcano, radial stress $d\Delta\sigma_y/dz$ values are highest, and

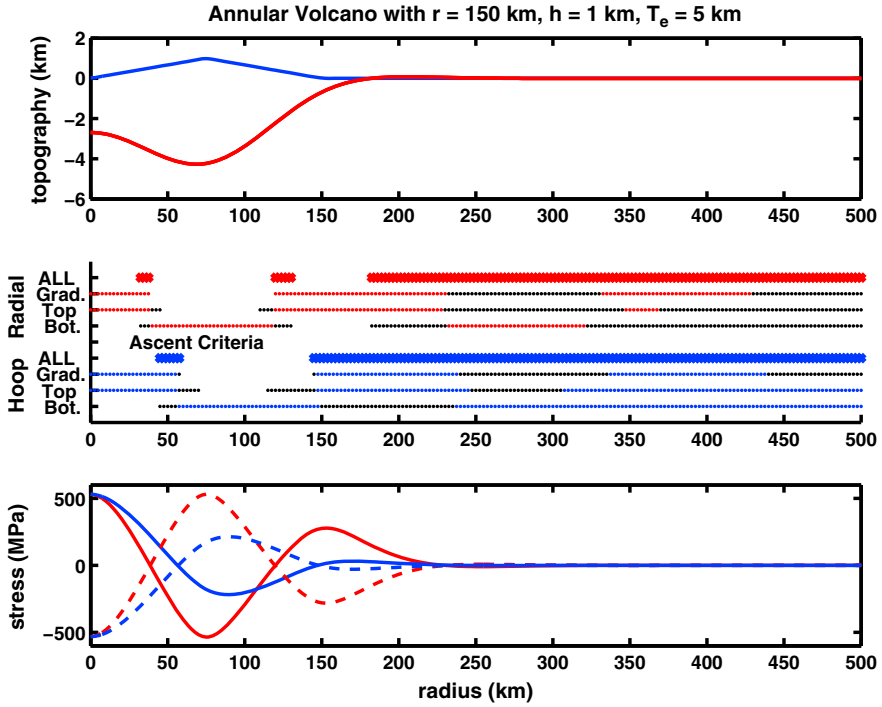

Figure 8. Flexure solutions versus radius for volcanoes with annular edifice, as in Figure 5, for $T_e = 5$ km.

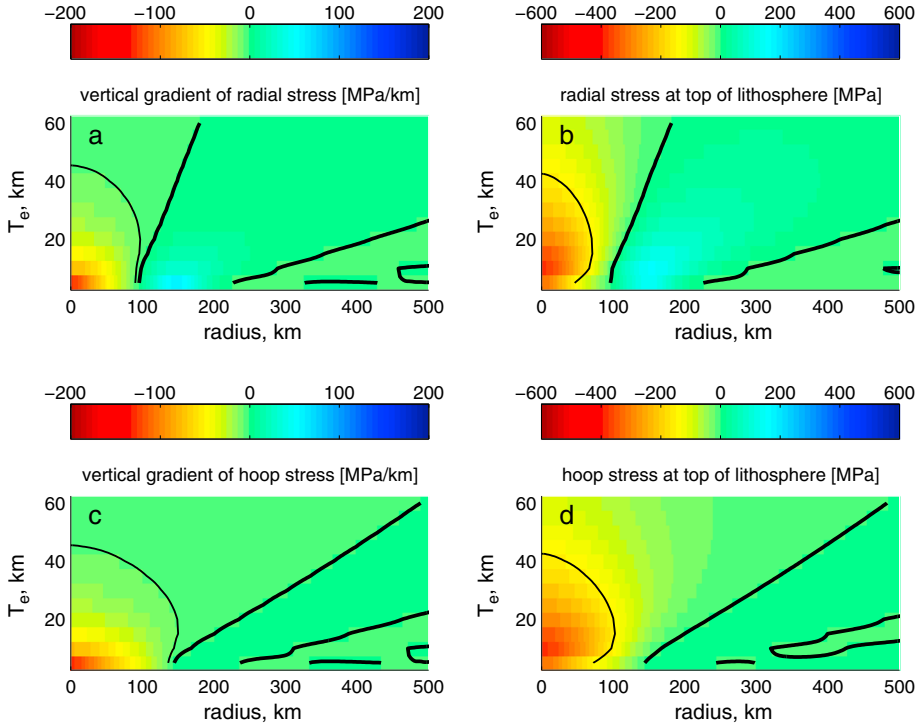

Figure 9. Maps of lithospheric stress gradients and stresses over the parameter space T_e versus radius, for conical edifice with $r_{ed} = 150$ km and $h_{ed} = 1$ km. Thin contours are shown at -6 MPa/km for stress gradients and -150 MPa for stress (corresponding to the thresholds for these quantities), thick contours are shown at values of 0 for these quantities. (a) Stress gradient for radial normal stress $d\sigma_{rr}/dz$. (b) Radial normal stress σ_{rr}. (c) Stress gradient $d\sigma_{\theta\theta}/dz$ for tangential normal stress. (d) Tangential normal stress $\sigma_{\theta\theta}$.

therefore most favorable for ascent, in a narrow band centered at about $r = 150$ km, at the lowest values of T_e shown (Figure 9a). Radial stresses at the top of the lithosphere show high positive magnitudes in roughly the same range of r and T_e (Figure 9b). However, the entirety of this region is not necessarily favorable for magma ascent because the stresses at the bottom of the lithosphere have the same high magnitude but opposite sign, thereby violating the stress ascent criterion there. To satisfy the ascent criteria throughout the depth of the lithosphere (within the allowable threshold), stress magnitudes need to be low. Thus, in Figure 9b, the most likely ascent regions are those close to the (thick) zero contours (i.e., within threshold σ_{local}); for $\sigma_{local} = 150$ MPa, $T_e \geq 50$ km is required to allow magma ascent throughout the full range of r, including the center. Note that because stresses are essentially symmetric about the neutral plane, the zero contours for both stress and $d\Delta\sigma_y/dz$ are virtually identical. For tangential stresses (Figure 9, bottom row), the overall situation is similar to the radial stress cases, except that favorable distal stress gradients are smaller in magnitude, and the central zones of unfavorable stress and $d\Delta\sigma_y/dz$ are wider.

[20] Results for domical edifices (Figure 10) are broadly similar to those for conical edifices. An apparent increase in $d\Delta\sigma_y/dz$ and stress magnitudes compared to Figure 8 is mostly attributable to the fact that a truncated cone of a given height has greater volume and mass than a cone of the same height. One substantive difference is the absence of adverse $d\Delta\sigma_y/dz$ and stress near the symmetry axis for the smallest values of T_e, a result of the lack of plate bending beneath the center of the truncated cone load (see Figure S6); at low T_e, the flexural response moves to the margin of the edifice. For an annular edifice, there is a further change in the stress near $r = 0$ (Figure 11), such that for low T_e, the region near now experiences positive $d\Delta\sigma_y/dz$ and lithosphere surface stress, thereby producing the inner ascent zones shown in Figure 8.

6. Discussion

6.1. Lithospheric Thickness and Edifice Shape

[21] Our results have strong implications for the generation and maintenance of volcanic edifice shapes on Venus. At high elastic thicknesses ($T_e > 50$ km), magma ascent criteria are met over a wide radius range that includes the center of a conical edifice (Figure 6). Presuming a magma source concentrated toward the central axis, direct ascent along such pathways would tend to produce an edifice also concentrated toward the center, i.e., a conical shape. For thinner elastic lithospheres, the region near the center of the cone experiences high $d\Delta\sigma_y/dz$ (throughout the thickness of the lithosphere) and compression (in the upper lithosphere), thereby shutting off magma ascent near the center of the edifice (Figures S3 and S5). This regime would tend to shut off summit eruptions and therefore halt construction of the central part of a cone; instead, flank eruptions would tend to build up the flanks at the expense of the center, thereby

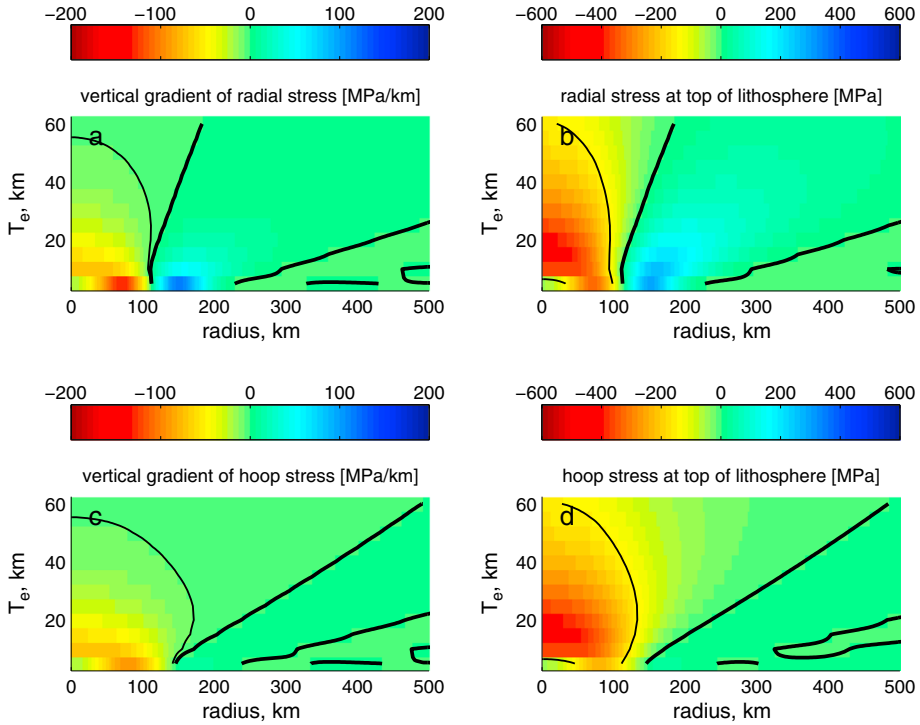

Figure 10. Maps of stress gradients and stresses, as in Figure 9, for truncated cone (domical) edifice.

producing a flat-topped edifice or dome. We find that this is consistent with model results for domical edifices at intermediate T_e values (around 25 km, Figure 7); eruptions from circumferential dikes are predicted on the outer flank of such edifices. Such eruptions would tend to reinforce the domical shape.

[22] At low T_e, (<= 10 km), conical and domical edifices returned extremely high magnitudes of negative stress gradients and compressive stresses near the top of the lithosphere; these conditions are inconsistent with the formation of such edifice shapes. However, annular edifices on thin lithosphere (Figure 8) exhibit two zones of allowed ascent; one on the

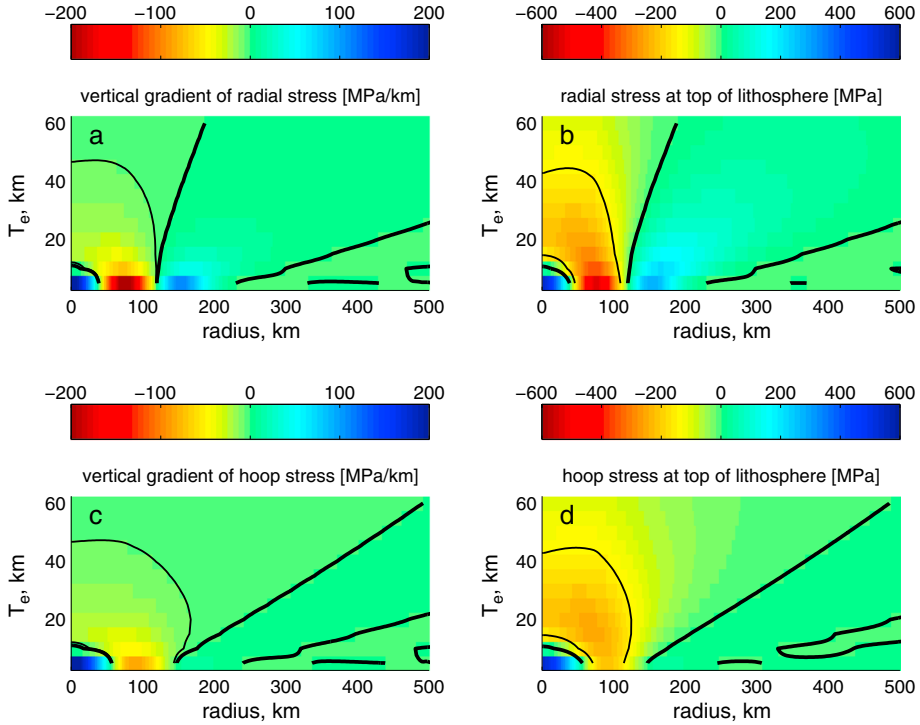

Figure 11. Maps of stress gradients and stresses, as in Figure 9, for annular edifice.

inside of the ridge and one on the outside. The short wavelength response of thin lithospheres tends to produce very narrow zones of magma ascent (Figure 8). This configuration is broadly consistent with long-term maintenance of an annular shape, although radial migration of the eruption centers in response to the growing load is likely and necessary to produce single (rather than paired) annulus. Models of annular edifices emplaced on very thick lithospheres (Figure S2) predict ascent everywhere, requiring a very fortuitous pattern of sublithosphere magma accumulation (essentially, a torus) to generate the observed topography. On intermediate lithospheres (Figure S4), annular loads generate a central cutoff that is more consistent with a domical (e.g., Figure 7), rather than annular, shape. Thus, we argue that annular edifices are the most likely expression of volcanic edifice construction at low T_e (provided that the loading is slow with respect to the relaxation time in the ductile mantle, see below).

[23] This switch from negative to positive $d\Delta\sigma_y/dz$ gradient at the center of annular loads for low T_e illustrates an interesting property of the ascent criteria. In principle, once flexure starts, the stress orientation criterion is always violated at some depth in the lithosphere, because the stress versus depth profile tends to be symmetric about the midplane of the lithosphere; as pointed out above, half of the lithosphere is always in compression. In practice, however, we argue that the mitigating factors outlined above (σ_{local} from equation (1) and ΔPG from equation (4)) are sufficient to reorient the principal stresses where differential stress magnitudes are small. Furthermore, in situations where $d\Delta\sigma_y/dz$ is very positive (e.g., the $T_e = 5$ km case in Figure 8), the high gradient inevitably produces very highly compressive $\Delta\sigma_y$ in the lower lithosphere. Thus, the two criteria tend to be antagonistic: A very favorable value for one criterion tends to yield a very unfavorable one for the other. Magma ascent therefore tends to occur where the values for both stresses and stress gradients are small in magnitude, but within the allowances set by σ_{local} and ΔPG. A similar conclusion was reached (through different physical reasoning) by *Hieronymus and Bercovici* [2001a, 2001b].

[24] Our results have implications for the timing of edifice construction. The mantle's viscoelastic response to loading has a characteristic timescale, called the Maxwell time, given by $\tau_M = \eta/(2\,E)$, where η is viscosity and E is Young's modulus. At times short compared to τ_M, the lithospheric response, and therefore the flexural stresses, is negligible. The stress state would simply be the prevolcanism state, which we presume would be within the limits of the stress and gradient thresholds described above; thus, ascent would be allowed everywhere. Given a centrally concentrated magma source, we might expect an initially conical or domical edifice to form. Potentially, if the magma flow rate were rapid enough, an entire edifice could be emplaced before stresses from the flexural response could shut off central ascent paths. Such volcanoes resemble the "instantaneous load" case of *McGovern and Solomon* [1993] and would be expected to exhibit strong compressional faulting at the surface. In general, such faulting has not been reported at large volcanoes on Venus [e.g., *Crumpler et al*., 1997], suggesting that the high flow rates required were not generated. However, it might be difficult to detect such faults in the absence of high-resolution topography for Venus: The extent of compressional faulting on large volcanoes on Mars was not fully recognized until revealed by high-resolution Mars Orbiter Laser Altimeter topography [e.g., *Byrne et al*., 2009, 2013].

[25] If Venus volcanoes are not forming as essentially "instantaneous loads", then lithospheric stresses may be controlling not just their shapes but also their heights. After reaching a certain height, central magma ascent will be shut down. If the magma supply zone is narrower than the width of the shutdown region, the magma will not be able to reach flank ascent zones, and the volcano will cease growing extrusively (intrusive growth is still possible, see below) rather than transform into a domical volcano. Such a scenario may in part account for the relatively low average heights of volcanoes on Venus relative to those on Mars, where thicker lithospheres [e.g., *McGovern et al*., 2002, 2004; *Belleguic et al*., 2005] and lower gravity allow much taller edifices to form.

[26] The models presented above have been interpreted in terms of direct ascent paths from a mantle melt source to the surface, but paths that involve horizontal transport, via sill-like intrusions in the lithosphere [e.g., *Solomon and Head*, 1979, 1980] or flow at the base of the lithosphere [*Sparks and Parmentier*, 1991; *Montési et al*., 2011] are also possible. *McGovern et al*. [2001] proposed that compressive stresses in the upper lithosphere generate a broad zone of sill intrusion within the Martian volcano Alba Patera; inflation in turn produces an annular extensional fault zone on the rim of that domical edifice. This zone may be enhanced by the surface expression of dikes rising from the outer margin of the sill complex. For a stress state like that in Figure 7, two factors inhibit central magma ascent: horizontal compression in the upper lithosphere and a large negative stress gradient throughout it. In practice, early inflation of dikes may counteract the nascent extensional stress state in the lower lithosphere [e.g., *Hieronymus and Bercovici*, 2001a, 2001b; *Pritchard et al*., 2006; *McGovern*, 2007], thereby reducing the effect of the adverse stress gradient. However, the adverse stress orientations in the upper lithosphere would still prevent dike formation, instead resulting in subhorizontal sills.

6.2. Application to Specific Volcanic Edifices on Venus

[27] Sif Mons is an example of a conical edifice (Figure 1a). The stress states for loading of a thick lithosphere (Figure 6) allow ascent in both radial and circumferential dike geometries over the entire edifice, consistent with the prominent presence of flow units covering the edifice. Regional-scale considerations, such as preexisting structure (e.g., the Guor Linea rift exposed on the other side of the Western Eistla rise [*Grimm and Phillips*, 1992]), regional stress variations, or late-stage uplift [e.g., *McGovern et al*., 2001] may account for the preference for radial orientation of fractures in the flow apron of Sif Mons (if indeed, they are related to edifice growth). The relative paucity of tectonic structures on the upper flanks of the edifice (Figure 1a) suggests that magma supply rate may have overwhelmed tectonic deformation in the recent history of the volcano.

[28] Kokyanwuti Mons exemplifies the "truncated cone" or domical edifice shape (Figure 4), for which emplacement at intermediate T_e is indicated (Figure 6). The locations of the observed caldera, flow, and fracture systems at or below the slope break of the central flat summit region are

consistent with the scenario outlined above for a domical edifice at intermediate T_e (Figure 5b), magma ascent at the margins of the edifice in conduits with circumferential geometry. In particular, the proposed caldera appears to be the center of the youngest unit of volcanic flows (Figure 2) and thus representative of the most recent interactions of stress and magma ascent in Kokyanwuti Mons.

[29] The annular shapes of Aruru Corona's topography and fracture system (Figures 3 and 4) are distinguishing marks of the morphologic class corona. The annular load model of Figure 7 ($T_e = 5$ km) predicts zones of magma ascent on both the inner and outer flanks, consistent with the observed distribution of flows on Aruru (Figure 3), in particular the inward-directed flows in the center (unit *l2*). Furthermore, the model predicts two subzones of dike-transported ascent on the outer flanks: an upper zone with predicted circumferential dike orientations (caused by radial stresses) and a lower zone of predicted radial orientations (from the hoop stresses). This is consistent with the observed distribution of fractures on Aruru, especially the tendency for the radial fractures to extend further down the slopes to the north and south. Our result is similar to the best fit T_e value of 10 km determined by *Rumpf and McGovern* [2007] based on topographic profiles of Aruru and the observed tectonic and flow distributions. Our result is also consistent with the $T_e = 0$–7 km estimate from gravity/topography admittance for a top-loaded (i.e., appropriate for a constructed edifice) model of Aruru [*Hoogenboom et al*., 2004]. A majority of coronae investigated by these authors with a top-loading model had a lower bound of 0 for T_e, consistent with very thin lithosphere. Interestingly, almost all coronae with lower bounds on T_e greater than 0 from top-loading analysis occur in the "fracture belt" geologic setting [*Hoogenboom et al*., 2004], suggesting that coronae in such settings may form by a different mechanism than the constructional one proposed here.

6.3. Some Coronae are Strangely Shaped (Annular) Volcanoes

[30] Above, we show that annular loads produce a distinct effect on the flexural stress state within the lithosphere, such that for thin lithospheres, the annular shape tends to be reinforced by the resulting pattern of magma ascent (Figure 5c). This finding yields a new model for corona formation via stress-regulated volcanic construction. Here we suggest that the subset of coronae that have significant annular ridge topography, abundant lava flows associated with that topography, and a gravity signature consistent with low T_e are formed primarily via volcanic construction. In other words, such coronae are essentially strangely shaped volcanic edifices. This model is in principle similar to several previous models of surface corona loads [e.g., *Janes et al*., 1992; *Cyr and Melosh*, 1993; *Janes and Squyres*, 1995] but is the first to explicitly account for the interactions of lithospheric flexure, magma ascent, and edifice growth.

[31] Coronae lacking substantial positive relief, exhibiting primarily negative relief, and/or lacking evidence for a really significant lava flows may not have formed by this constructional mechanism. Such coronae constitute a significant fraction of the total number [e.g., *Smrekar and Stofan*, 1997]. Inferences of very large values of T_e at specific coronae from gravity measurements [e.g., *Hoogenboom et al*., 2004] are also inconsistent with this mechanism, although gravity-based inferences are nonunique and correspond to present conditions, not necessarily those at the time of corona formation.

[32] T_e estimates for coronae show wide variations, but many volcanic coronae fit with a surface-loading (i.e., volcanic construction) model have low T_e [*Hoogenboom et al*., 2004]. Bottom-loading models tend to give much higher estimates for T_e [*Hoogenboom et al*., 2004, 2005]; such models may indicate postformation mantle dynamics beneath coronae, consistent with the finding of *Hoogenboom et al*. [2005] that younger coronae associated with chasmata exhibit smaller values of T_e than coronae that predated chasmata formation. Furthermore, as corona diameter increases, the transition value for T_e to behave as "thin" increases [e.g., *McGovern and Solomon*, 1998] because the flexural wavelength is also increasing. Thus, relatively high values of T_e at very large coronae [e.g., *Johnson and Sandwell*, 1994] are not necessarily inconsistent with the scenario proposed here, although the prominent contributions of tectonics to the construction of larger coronae may point to a different formation mechanism.

[33] Volcanically constructed coronae may have more in common with more conventional volcanic edifices than with corona formed by deformation from subsurface flow mechanisms [e.g., *Janes et al*., 1992; *Koch and Manga*, 1996; *Smrekar and Stofan*, 1997; *Hansen*, 2003; *Hoogenboom and Houseman*, 2006]. This idea is consistent with the identification of volcano-corona "hybrid" structures [e.g., *McGill*, 1998; *Grindrod et al*., 2006], although we would argue that the term "hybrid" is unnecessary if some coronae are mainly constructed volcanically as proposed here. Further, there is likely a continuum of processes that contribute to the wide range of corona morphologies seen on Venus, and a given structure may be the result of combined construction, intrusive magmatism [e.g., *McGovern et al*., 2001; *Dombard et al*., 2007], and subsurface flow. A common assumption in the literature is that all features termed corona are formed by one mechanism [e.g., *Smrekar and Stofan*, 1997; *Hoogenboom and Houseman*, 2006; *Dombard et al*., 2007]. This assumption is then applied as a criterion with which to evaluate models for corona formation, along the lines of "A successful model of corona formation must simultaneously explain X, Y and Z", with X, Y, and Z being properties of the entire set of objects designated as coronae or subsets of them. In light of the diversity of potential corona formation mechanisms, the prevailing (and often unspoken) assumption that "There can be only one" may lead to the improper dismissal of corona formation models which only apply to a subset of coronae (like the one proposed here). It may also skew analyses of coronae that formed are by viscous flow or other mechanisms. In other words, it is safer to view the term corona as descriptive rather than genetic.

6.4. Inferences of Regional and Global Thermal History From Volcanic Edifice Shapes

[34] Our results also have implications for regional thermal history on Venus. Eistla Regio on Venus comprises several concentrations of volcanic activity. Western Eistla Regio consists of a broad topographic rise superposed by the conical shield volcanoes Sif and Gula Montes [*Grimm and Phillips*, 1992]. In Central Eistla Regio, the volcanoes Anala Mons and Irnini Mons lie in close proximity. While Anala has a domical profile, Irnini Mons exhibits an annular topographic

ridge with associated circumferential tectonics. An early name for the center of Irnini Mons is Sappho Patera, for which the map quadrangle is named [*McGill*, 2000] and which was reckoned as a corona [*Stofan et al*., 1992]. Eastern Eistla Regio encompasses four large corona structures.

[35] Edifice shapes in Eistla Regio appear to systematically change with distance to the east. The Western Eistla edifices Sif and Gula Montes have conical edifices that are consistent with emplacement on thick lithosphere (high T_e). The domical shape of Anala Mons in Central Eistla suggests emplacement at moderate T_e, and the annular Irnini Mons edifice and Eastern Eistla coronae is consistent with emplacement at low T_e. This trend can be accounted for in several ways. If volcanic edifice construction in Eistla Regio is more or less coeval, a gradient in lithospheric thickness (decreasing to the east) is indicated. Alternatively, in the context of a planet cooling down after a more or less catastrophic resurfacing event, the edifices may get younger toward the west. Such a hypothesis is difficult to test on a broad scale, since Western and Central Eistla are too far apart to have direct stratigraphic contact, and the cratering record is too sparse to constrain ages of individual constructs. However, mapping of Central Eistla indicates that Irnini Mons is older than Anala Mons [*McGill*, 2000]. In the context of the elevated thermal profiles expected from a wide-scale catastrophic resurfacing event [e.g., *Schubert et al*., 1997], this age relationship is consistent with the idea that Irnini formed during an older, hotter (thinner lithosphere) period. Our findings thus support the idea that lithospheric cooling helped to bring on a transition between emplacement of annular edifices (e.g., Irnini Mons) and younger domical or conical ones [*McGovern and Solomon*, 1998; *McGill*, 1994].

[36] Finally, our results also have implications for global thermal history. While the impact crater population on Venus does not allow individual volcanic constructs to be dated, grouping all features of a given type into one global "unit" allows the global average ages of different types of features to be compared. Such analysis reveals that shield volcanoes (including the "conical" and "domical" edifice types studied here) on average have surface ages less than those of coronae ("annular" edifice type) [*Namiki and Solomon*, 1994; *Price and Suppe*, 1994]. Again, such a result is consistent with our findings on lithospheric thickness and edifice shape in the context of a lithosphere that is cooling after a catastrophic resurfacing event.

6.5. Applications to Other Planets

[37] On Mars, no fully annular shaped edifices have been observed, although the feature called Acheron Fossae comprises a half annulus of the elevated and faulted terrain, partially buried by the moat-filling deposits and aureole of Olympus Mons. However, the two very large volcanic rises, Alba Mons (formerly Alba Patera) and the Elysium Rise, have domical shapes with fractures (graben) at and emanating from the margins of their flat summits, particularly well developed in the case of Alba Mons [e.g., *McGovern et al*., 2001]. Their shapes, tectonic signatures, and lava flow patterns are consistent with the intermediate T_e scenario described above. The same compressive stresses that help to create the central magma ascent shutoff (e.g., Figure 5b) will direct lateral magma propagation in sill-like bodies, the inflation of which generates annular fault zones at the sill margins [*McGovern et al*., 2001]. Because of its tectonic fault annulus, Alba Mons has been suggested as an analog to coronae on Venus [e.g., *Watters and Janes*, 1995]. This is a reminder that the classification corona comprises both annular and domical or plateau topography [e.g., *Smrekar and Stofan*, 1997], and thus, some Venusian coronae likely fall under the domical, intermediate-thickness lithosphere category of our models. The fracture annuli for domical coronae on Venus may be produced by inflation of an intrusive sill complex, driven by the highly compressive stress state in the central upper lithosphere, as proposed for Alba Mons on Mars by *McGovern et al*. [2001]. The Arsia Mons volcano has a broad, flat caldera region and many circumferential graben on its lower flanks, also consistent with the topography and stress predicted for the intermediate T_e scenario. Taller, more conical edifices like Olympus and Ascraeus Montes suggest emplacement at larger T_e. These relationships are consistent with the relative estimates of T_e for these volcanoes derived from gravity/topography relationships [*McGovern et al*., 2002, 2004; *Belleguic et al*., 2005].

[38] It has been argued that there are no analogs to corona features on Earth [e.g., *Smrekar and Stofan*, 1997]. By the scenarios proposed here, any such volcanoes would have to be emplaced on low- (or, for domical edifices with fault annuli, intermediate-) thickness lithosphere. On Earth, plate tectonics dictate that such settings occur on the youngest oceanic lithosphere, at or near mid-ocean ridges [see also *Watters and Janes*, 1995]. Plume-induced volcanism on or close to mid-ocean ridges (that is to say, volcanism above and beyond that normally associated with ridge spreading) is strongly affected by the structure of the ridge itself, resulting in constructs that conform to the shapes of ridge and transform faults (e.g., the Azores) or lack circular/annular symmetry and structure (e.g., Iceland). Any such symmetry is likely destroyed by the spreading process. Thus, we must look off ridge for evidence of lithosphere-volcano interactions of the type described above. The volcanoes of the Galapagos chain, located very close to but not on the Cocos-Nazca ridge, may provide the best examples of such interactions. T_e is low in the region, about 6 km in the eastern/central archipelago and 12 km beneath the western Galapagos volcanoes [*Feighner and Richards*, 1994]. The distribution of the western Galapagos shields, the "J-shaped" Isla Isabella comprising six edifices and the lone edifice of Isla Fernandina occupying the space above the hook of the "J", can be interpreted to define an annulus, albeit highly distorted by the tectonic fabric of the young oceanic crust there. Thus, the volcanoes of the western Galapagos may define a meta corona.

7. Conclusions and Future Work

[39] We have applied two types of stress-based magma ascent criteria to modeled stress states for conical-, domical-, and annulus-shaped volcanoes at a range of elastic lithosphere thickness T_e values. In summary, there appears to be a preferred range of T_e for each edifice shape. High T_e results in low magnitudes of ascent-adverse stresses and stress gradients, allowing conical edifices with flows originating from anywhere on the edifice. Our results support the finding of *McGovern and Solomon* [1998] that thick elastic lithospheres facilitate the growth of large conical edifices. At intermediate

values of T_e, high adverse stress gradients throughout the lithosphere and compressive stresses in the lower lithosphere cut off magma ascent near the central axis of a conical edifice. Ascent is possible only on the lower flanks, thereby promoting lower flank growth at the expense of summit eruptions, resulting in a more domical topographic profile. At the lowest values of T_e, high stresses cut off central magma ascent for both conical and domical edifices, but the "form-fitting" flexural response to an annular load results in narrow, spaced zones of allowed magma consistent with the annular topography.

[40] This paper presents a purely surface-loading scenario that accounts for the shape and tectonic signatures associated with volcanic edifices of varying shapes. In particular, it provides an alternative formation model of volcano-tectonic constructs with annular topographic and/or tectonic signatures called coronae. Previous models for their formation invoke substantial broad-scale subsurface loading from viscous or diapiric mechanisms. It is likely that a broad range of loading mechanisms contribute to the observed suite of volcano-tectonic features with annular topographic or tectonic signatures (e.g., "coronae"). Nonetheless, the success of our models in generating realistic topographic, tectonic, and growth histories for actual Venusian edifices suggests that scenarios dominated by volcanic construction and elastic/brittle deformation of the lithosphere may account for a significant fraction of edifices of all shapes on that planet.

[41] Here we have assumed the final shape of the edifices. Models that apply the ascent criteria to incremental batches of magma to determine where they may be emplaced (i.e., to determine the subsequent shape of the load) can lead to a more detailed understanding of the interactions between load shape and magma ascent. Preliminary results for such self-consistent models of edifice growth [*Buz and McGovern*, 2010] support our finding that T_e (along with edifice construction rate) exerts control of edifice shape, in a progression of conical to domical to annular edifices with decreasing T_e (and decreasing construction rate). Finally, for loads large with respect to the planetary radius, membrane stresses from lithospheric stretching come into play. Such stresses, constant through the thickness of the lithosphere, can shift the lithosphere into extension in regions beyond the margins of large downward loads [e.g., *Litherland and McGovern*, 2009]. This can counter the effects of compression in parts of the lithosphere, enhancing magma ascent and facilitating the formation of volcanic edifices and provinces [e.g., *Spudis et al*., 2013]. Consideration of such stresses may enhance efforts to understand the evolution of the largest volcanoes on Venus.

[42] **Acknowledgments.** We thank Patricia Gregg, an anonymous reviewer, and Associate Editor David Baratoux for helpful comments. This research was supported by NASA Planetary Geology and Geophysics (PG&G) grants NNG05GJ92G, NNX08AL77G, and NNX12AO49G. This is LPI Contribution number 1762.

References

Anderson, E. M. (1951), *The Dynamics of Faulting and Dyke Formation With Application to Britain*, Oliver and Boyd, Edinburgh.

Belleguic, V., P. Lognonné, and M. Wieczorek (2005), Constraints on the Martian lithosphere from gravity and topography data, *J. Geophys. Res.*, *110*, E11005, doi:10.1029/2005JE002437.

Borgia, A. (1994), Dynamical basis of volcanic spreading, *J. Geophys. Res.*, *99*, 17,791–17,804.

Buz, J., and P. McGovern (2010), Venusian volcano shapes: Implications for edifice evolution and the internal thermal state of Venus, Abstract # 1482 (CD-ROM), LPSC XLI.

Byrne, P. K., B. van Wyk de Vries, J. B. Murray, and V. R. Troll (2009), The geometry of volcano flank terraces on Mars, *Earth Planet. Sci. Lett.*, *281*, 1–13.

Byrne, P. K., E. P. Holohan, M. Kervin, B. van Wyk de Vries, V. R. Troll, and J. B. Murray (2013), A sagging-spreading continuum of large volcano structure, *Geology*, *41*, 339–342.

Chadwick, W. W., Jr., and K. A. Howard (1991), The pattern of circumferential and radial eruptive fissures on the volcanoes of Fernandina and Isabela islands, Galapagos, *Bull. Volcanol.*, *53*, 259–275.

Comer, R. P. (1983), Thick plate flexure, *Geophys. J. R. Astron. Soc.*, *72*, 101–113.

Copp, D. L., and J. E. Guest (2007), Geologic Map of the Sif Mons Quadrangle (V-31), Venus, USGS Scientific Investigations Map I-2898.

Crumpler, L. S., J. C. Aubele, D. A. Senske, K. P. Magee, and J. W. Head (1997), Volcanoes and centers of volcanism on Venus, in *Venus II*, pp. 1362 , University of Arizona Press, Tucson.

Cyr, K. E., and H. J. Melosh (1993), Tectonic patterns and regional stresses near Venusian coronae, *Icarus*, *102*, 175–184.

Dombard, A. J., C. L. Johnson, M. A. Richards, and S. C. Solomon (2007), A magmatic loading model for coronae on Venus, *J. Geophys. Res.*, *112*, E04006, doi:10.1029/2006JE002731.

Feighner, M. A., and M. A. Richards (1994), Lithospheric structure and compensation mechanisms of the Galapagos Archipelago, *J. Geophys. Res.*, *99*, 6711–6729.

Ford, P. G., and G. H. Pettengill (1992), Venus topography and kilometer-scale slopes, *J. Geophys. Res.*, *97*, 13,103–13,114.

Galgana, G. A., P. J. McGovern, and E. B. Grosfils (2011), Evolution of large Venusian volcanoes: Insights from coupled models of lithospheric flexure and magma reservoir pressurization, *J. Geophys. Res.*, *116*, E03009, doi:10.1029/2010JE003654.

Galgana, G. A., E. B. Grosfils, and P. J. McGovern (2013), Radial dike formation on Venus: Insights from models of uplift, flexure and magmatism, *Icarus*, *225*, 538–547.

Grimm, R. E., and R. J. Phillips (1992), Anatomy of a Venusian hot spot—Geology, gravity, and mantle dynamics of Eistla Regio, *J. Geophys. Res.*, *97*, 16,035–16,054.

Grindrod, P. M., E. R. Stofan, A. W. Brian, and J. E. Guest (2006), The geological evolution of Atai Mons, Venus: A volcano-corona 'hybrid', *J. Geol. Soc. London*, *163*, 265–275.

Grosfils, E. B. (2007), Magma reservoir failure on the terrestrial planets: Assessing the importance of gravitational loading in simple elastic models, *J. Volcanol. Geotherm. Res.*, *166*, 47–75.

Gudmundsson, A. (2002), Emplacement and arrest of sheets and dykes in central volcanoes, *J. Volcanol. Geotherm. Res.*, *116*, 279–298.

Gudmundsson, A. (2006), How local stresses control magma-chamber ruptures, dyke injections, and eruptions in composite volcanoes, *Earth Sci. Rev.*, *79*, 1–31.

Hansen, V. L. (2003), Venus diapirs: Thermal or compositional, *GSA Bull.*, *115*, 1040–1052.

Head, J. W., L. S. Crumpler, J. C. Aubele, J. E. Guest, and R. S. Saunders (1992), Venus volcanism: Classification of volcanic features and structures, associations, and global distribution from Magellan data, *J. Geophys. Res.*, *97*, 13,153–13,197.

Hieronymus, C. F., and D. Bercovici (2001a), Focusing of eruptions by fracture wall erosion, *Geophys. Res. Lett.*, *9*, 1823–1926.

Hieronymus, C. F., and D. Bercovici (2001b), A theoretical model of hotspot volcanism: Control on volcanic spacing and patterns via magma dynamics and lithospheric stress, *J. Geophys. Res.*, *106*, 683–702.

Hoogenboom, T., and G. A. Houseman (2006), Rayleigh Taylor instability as a mechanism for corona formation on Venus, *Icarus*, *180*, 292–307.

Hoogenboom, T., S. E. Smrekar, F. S. Anderson, and G. Houseman (2004), Admittance survey of type I coronae on Venus, *J. Geophys. Res.*, *109*, E03002, doi:10.1029/2003JE002171.

Hoogenboom, T., G. Houseman, and P. Martin (2005), Elastic thickness estimates for coronae associated with chasmata on Venus, *J. Geophys. Res.*, *110*, E09003, doi:10.1029/2004JE002394.

Hurwitz, D. M., S. M. Long, and E. B. Grosfils (2009), The characteristics of magma reservoir failure beneath a volcanic edifice, *J. Volcanol. Geotherm. Res.*, *188*, 379–394.

Ito, G., and S. J. Martel (2002), Focusing of magma in the upper mantle through dike interaction, *J. Geophys. Res.*, *107*(B10), 2223, doi:10.1029/2001JB000251.

Janes, D. M., and S. W. Squyres (1995), Viscoelastic relaxation of topographic highs on Venus to produce coronae, *J. Geophys. Res.*, *100*, 21,173–21,188.

Janes, D. M., S. W. Squyres, D. L. Bindschadler, G. Baer, G. Schubert, V. L. Sharpton, and E. R. Stofan (1992), Geophysical models for the formation and evolution of coronae on Venus, *J. Geophys. Res.*, *97*, 16,055–16,068.

Johnson, C. L., and D. T. Sandwell (1994), Lithospheric flexure on Venus, *Geophys. J. Int.*, *119*, 627–647.

Koch, D. M., and M. Manga (1996), Neutrally buoyant diapirs: A model for Venus coronae, *Geophys. Res. Lett.*, (23), 225–228.

Lister, J. R., and R. C. Kerr (1991), Fluid-mechanical models of crack propagation and their application to magma transport in dykes, *J. Geophys. Res.*, *96*, 10,049–10,077.

Litherland, M. M., and P. J. McGovern (2009), Effects of planetary radius on lithospheric stresses and magma ascent on the terrestrial planets, Lunar Planet. Sci., 40, abstract 2201.

Long, S. M., and E. B. Grosfils (2009), Modeling the effect of layered volcanic material on magma reservoir failure and associated deformation, with application to Long Valley caldera, California, *J. Volcanol. Geotherm. Res.*, (186), 349–360.

McGill, G. E. (1994), Hotspot evolution and Venusian tectonic style, *J. Geophys. Res.*, *99*, 23,149–23,161.

McGill, G. E. (1998), Central Eistla Regio: Origin and relative age of topographic rise, *J. Geophys. Res.*, *103*, 5889–5896.

McGill, G. E. (2000), Geologic map of the Sappho Patera Quadrangle (V-20), Venus, U.S. Geological Survey Geologic Investigations Series Map I-2637.

McGovern, P. J. (1996), Studies of large volcanoes on the terrestrial planets: Implications for stress state, tectonics, structural evolution, and moat filling, PhD thesis, 339 pp., Mass. Inst. of Technol., Cambridge.

McGovern, P. J. (2007), Flexural stresses beneath Hawaii: Implications for the October 15, 2006, earthquakes and magma ascent, *Geophys. Res. Lett.*, *34*, L23305, doi:10.1029/2007GL031305.

McGovern, P. J., and S. C. Solomon (1993), State of stress, faulting, and eruption characteristics of large volcanoes on Mars, *J. Geophys. Res.*, *98*, 23,553–23,579.

McGovern, P. J., and S. C. Solomon (1997), Filling of flexural moats around large volcanoes on Venus: Implications for volcano structure and global magmatic flux, *J. Geophys. Res.*, *102*, 16,303–16,318.

McGovern, P. J., and S. C. Solomon (1998), Growth of large volcanoes on Venus: Mechanical models and implications for structural evolution, *J. Geophys. Res.*, *103*, 11,071–11,101.

McGovern, P. J., S. C. Solomon, J. W. Head, D. E. Smith, M. T. Zuber, and G. A. Neumann (2001), Extension and uplift at Alba Patera, Mars: Insights from MOLA observations and loading models, *J. Geophys. Res.*, *106*, 23,769–23,809.

McGovern, P. J., S. C. Solomon, D. E. Smith, M. T. Zuber, M. Simons, M. A. Wieczorek, R. J. Phillips, G. A. Neumann, O. Aharonson, and J. W. Head (2002), Localized gravity/topography admittance and correlation spectra on Mars: Implications for regional and global evolution, *J. Geophys. Res.*, *107*(E12), 5136, doi:10.1029/2002JE001854.

McGovern, P. J., J. R. Smith, J. K. Morgan, and M. H. Bulmer (2004), The Olympus Mons aureole deposits: New evidence for a flank-failure origin, *J. Geophys. Res.*, *109*, E08008, doi:10.1029/2004JE002258.

Montési, L. G. J., M. D. Behn, L. B. Hebert, J. Lin, and J. L. Barry (2011), Controls on melt migration and extraction at the ultraslow Southwest Indian Ridge 10°–16° E, *J. Geophys. Res.*, *116*, B10102, doi:10.1029/2011JB008259.

Namiki, N., and S. C. Solomon (1994), Impact crater densities on volcanoes and coronae on Venus: Implications for volcanic resurfacing, *Science*, *265*, 929–933.

Pinel, V., and C. Jaupart (2003), Magma chamber behavior beneath a volcanic edifice, *J. Geophys. Res.*, *108*(B2), 2072, doi:10.1029/2002JB001751.

Pinel, V., and C. Jaupart (2004), Magma storage and horizontal dyke injection beneath a volcanic edifice, *Earth Planet. Sci. Lett.*, (221), 245–262.

Price, M., and J. Suppe (1994), Mean age of rifting and volcanism on Venus deduced from impact crater densities, *Nature*, *372*, 756–757.

Pritchard, M. E., A. M. Rubin, and C. J. Wolfe (2006), Do flexural stresses explain the mantle fault zone beneath Kilauea volcano?, *Geophys. J. Int.*, *168*, 419–430, doi:10.1111/j.1365-246X.2006.03169.x.

Rubin, A. M. (1995), Propagation of magma-filled cracks, *Annu. Rev. Earth Planet. Sci.*, *23*, 287–336.

Rumpf, M. E., and P. J. McGovern (2007), The influence of lithospheric flexure and volcano shape on magma ascent at large volcanoes on Venus, LPS XXXVIII, abstract 1374.

Saunders, R. S., et al. (1992), Magellan Mission Summary, *J. Geophys. Res.*, *97*, 13,067–13,090.

Schubert, G., V. S. Solomatov, P. J. Tackley, and D. L. Turcotte (1997), Mantle convection and the thermal evolution of Venus, in *Venus II*, edited by S. W. Bougher, D. M. Hunten, and R. J. Phillips, pp. 1245–1287, Univ. of Ariz. Press, Tucson.

Senske, D. A., G. G. Schaber, and E. R. Stofan (1992), Regional topographic rises on Venus: Geology of Western Eistla Regio and comparison to Beta Regio and Atla Regio, *J. Geophys. Res.*, *97*, 13,395–13,420.

Smrekar, S. E., and E. R. Stofan (1997), Corona formation and heat loss on Venus by coupled upwelling and delamination, *Science*, *277*, 1289–1294.

Solomon, S. C., and J. W. Head (1979), Vertical movement in mare basins: Relation to mare emplacement, basin tectonics, and lunar thermal history, *J. Geophys. Res.*, *84*, 1667–1682.

Solomon, S. C., and J. W. Head (1980), Lunar mascon basins: Lava filling, tectonics, and evolution of the lithosphere, *Rev. Geophys.*, *18*, 107–141.

Sparks, D. W., and E. M. Parmentier (1991), Melt extraction from the mantle beneath spreading centers, *Earth Planet. Sci. Lett.*, *105*(4), 368–377, doi:10.1016/0012-821X(91)90178-K.

Spudis, P. D., P. J. McGovern, and W. S. Kiefer (2013), Large shield volcanoes on the Moon, *J. Geophys. Res. Planets*, *118*, 1063–1081, doi:10.1002/jgre.20059.

Stofan, E. R., V. L. Sharpton, G. Schubert, G. Baer, D. L. Bindschadler, D. M. Janes, and S. W. Squyres (1992), Global distribution and characteristics of coronae and related features on Venus: Implications for origin and relation to mantle processes, *J. Geophys. Res.*, *97*, 13,347–13,378.

Stofan, E. R., J. E. Guest, and D. L. Copp (2001), Development of large volcanoes on Venus: Constraints from Sif, Gula and Kunapipi Montes, *Icarus*, *152*, 75–95.

ten Brink, U. S., and T. M. Brocher (1987), Multichannel seismic evidence for a subcrustal intrusive complex under Oahu and a model for Hawaiian volcanism, *J. Geophys. Res.*, *92*, 13, 687–13,707.

van Wyk de Vries, B., and R. Matela (1998), Styles of volcano-induced deformation: Numerical models of substratum flexure, spreading and extrusion, *J. Volcanol. Geotherm. Res.*, *81*, 1–18.

Watters, T. R., and D. M. Janes (1995), Coronae on Venus and Mars: Implications for similar structures on Earth, *Geology*, *23*, 200–204.

Wolfe, C. J., M. K. McNutt, and R. S. Detrick (1994), The Marquesas archipelagic apron: Seismic stratigraphy and implications for volcano growth, mass wasting, and crustal underplating, *J. Geophys. Res.*, *99*, 13,591–13,608.

Zahnle, K. J. (1992), Airburst origin of dark shadows on Venus, *J. Geophys. Res.*, *97*, 10,243–10,255.